Journal of Fluorescence
https://doi.org/10.1007/s10895-023-03351-8

RESEARCH

Synthesis and Characterisation of $SrAl_2O_4$: Eu^{3+} Orange-Red Emitting Nanoparticles

Neenu Mary Thomas[1,2,3] · **E I Anila**[2,4]

Received: 9 June 2023 / Accepted: 18 July 2023

Abstract
The current study involves the synthesis and characterisation of europium doped strontium aluminate nanophosphors using the solid-state reaction method with varying concentrations of europium. The existence of the $SrAl_2O_4$ phase in all samples was verified using X-ray diffraction and FTIR analysis. The lattice parameters as well as phase fractions were determined using Rietveld refinement. Surface morphology was studied using field emission scanning electron microscope. Using the Tauc plot method acquired from the diffuse reflectance spectra, the band gaps of the samples were determined and it was found that the doped samples possess lower band gaps compared to the host. Our findings demonstrate that these nanophosphors exhibiting bright orange-red emission under UV excitation with quantum efficiency 70.68%, can be applied for display and fluorescence imaging.

Keywords Nanophosphors · Strontium aluminate · Solid state reaction · Fluorescence · Quantum efficiency · Band gap

Introduction

Aluminates have been explored as the most suited host for creating persistent luminescent materials [1]. The exceptional optical properties of strontium aluminate based phosphor has made it an attractive candidate for diverse technological applications, including solid state lighting [2–4], optoelectronics [4], photocatalysis [5] and biomedical imaging [6]. Despite extensive research on strontium aluminate-based phosphors, research gaps still need to be addressed to understand and optimize their properties fully. One of the challenges in developing strontium aluminate based phosphors is achieving high luminescence efficiency, which depends on the synthesis method, dopant concentration, and particle size [1, 2]. Further investigation is needed to fully understand the electronic structure and optical properties of strontium aluminate based phosphors.

Solid state reaction [7], sol-gel method [8], combustion synthesis [9, 10], reflux method [11] are the most commonly used synthesis strategies to develop rare-earth doped strontium aluminates. The most used method for creating excellent phosphor materials is incorporating rare-earth ions as luminescent centers within an appropriate host material is conventional solid state reaction method. Literature suggests that attainment of single phase of strontium aluminate is possible only at high temperature sintering at $>=1200^0$ C [11–13]. Below this temperature range, mixed phases of strontium aluminates especially $SrAl_2O_4$, $Sr_3Al_2O_6$, $Sr_4Al_{14}O_{25}$ are formed. Even if the presence of more than one phases were reported, the effects due to coexistence of the phases were often neglected. Among the possible stable phases, $SrAl_2O_4$ with a large band gap ~ 6.6 eV [14] is the most studied host for luminescent material.

The activator rare earth ions are considered as the optical property deciding factor in nanophosphors. It is the transitions in their f-f, f-d levels, that gives the beneficial optical properties. Among the rare earth elements, europium (Eu) is considered to be best activator for red emission. Europium

✉ E I Anila
anila.ei@christuniversity.in

1 Department of Physics, Morning Star Home Science College, Angamaly, Kerala 683573, India

2 Optoelectronic and Nanomaterials' Research Lab, Department of Physics, Union Christian College, Aluva, Kerala 683102, India

3 Center for Nano-Bio Polymer Science and Technology, Department of Physics, St. Thomas College, Palai, Kerala 686574, India

4 Department of Physics and Electronics, Christ (Deemed to be University), Bangalore, Karnataka 560029, India

can exist in two ionised states namely Eu^{2+} and Eu^{3+}. Previous studies have reported the properties of $SrAl_2O_4$: Eu^{3+} nanophosphors obtained at a relatively low temperature of 1100^0 C with the existence of a minor phase, but these lack detailed in-depth analysis [3, 15–17].

Here we report, solid state synthesis of Eu^{3+} doped $SrAl_2O_4$ with varying concentrations of Eu^{3+} ions from 0 at% to 3 at% at 1100^0 C, along with comprehensive analysis of the structural and optical properties of the synthesised phosphors.

Experimental Details

Materials and Methods

Using analytical grade raw materials, the high-temperature solid-state reaction method was employed to synthesise undoped and europium doped strontium aluminate phosphor, namely strontium carbonate ($SrCO_3$, Merck, 99.95%), aluminium oxide (Al_2O_3, Merck, 99.95%) and europium (III) nitrate hydrate($Eu(NO_3)_3 \cdot 6H_2O$, Sigma Aldrich, 99.99%). The preparation of $Sr_{1-x}Al_2O_4$:xEu^{3+} phosphor (x = 0 at%, 0.5at. %, 1at. %, 1.5 at%, 2 at%, 2.5at. %, 3at. %) began with the precise weighing of raw materials based on their nominal compositions. Before synthesis, the precursor compounds were stoichiometrically weighed and subjected to a thorough mixing and milling procedure using an agate mortar and pestle for 2 h. The prepared sample was loaded into an alumina crucible and subsequently subjected to firing in air for 5 h at the specified temperature of 1100 °C. After cooling in the programmable furnace and performing additional grinding, the samples were obtained.

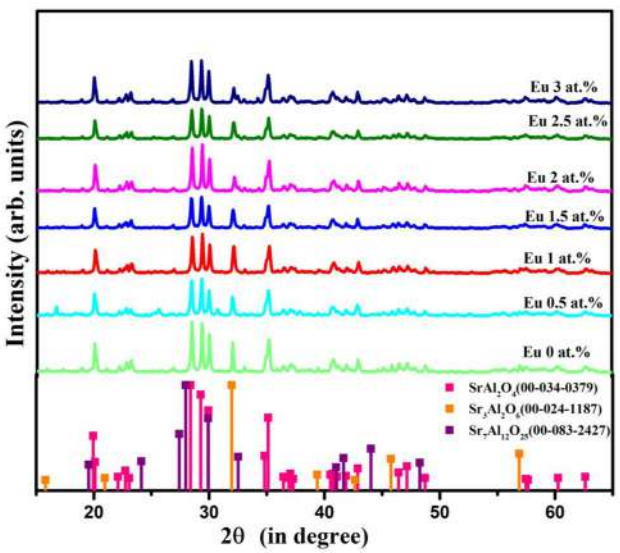

Fig. 1 X-Ray diffraction patterns obtained for $Sr_{1-x}Al_2O_4$:x Eu(x = 0 at% − 3 at%) nanophosphors

A benchtop powder X-ray diffractometer (Aeris Research, PANalytical) was utilized to thoroughly analyse and identify the crystalline phases of the synthesised samples. The diffractometer was operated with Cu Kα radiation (λ = 1.54 Å) and scanned within a range of 2θ = 10° − 90°. The surface morphology of the selected samples were performed by a FESEM (Apero 2 SEM, ThermoFisher Scientific). Fourier transform infrared (FTIR) spectra were acquired using a Perkin Elmer Spectrum Two FTIR Spectrometer through an attenuated total reflection (ATR) contact sampling method to delve deeper into the structural properties of the samples at room temperature. The spectra were collected within the range of 400 − 4000 cm^{-1}. The optical characteristics of the samples were evaluated by recording diffuse reflectance spectra with a Shimadzu UV-2600 UV-VIS-NIR spectrophotometer and performing photoluminescence analysis using a Horiba Fluoromax-4 C spectrofluorometer. The spectra were recorded by adjusting the excitation and emission slits to a width of 3 nm and integration time of 0.1 s. The quantum efficiency of the optimised sample were determined using the Edinburgh FLS1000 combined steady state and phosphorescence lifetime spectrometer.

Results and Discussion

Structure and Morphology

The powder X-ray diffraction (PXRD) patterns of synthesised samples of $Sr_{1-x}Al_2O_4$:x Eu^{3+}(x = 0 at% − 3 at%) are shown in Fig. 1. All the dominant X-ray diffraction peaks observed at $2\theta = 19.95^0$, 28.38^0, 29.27^0, 29.91^0 and 35.14^0 match well with standard file No. 00-034-0379, which are ascribed to the reflections from crystallographic planes (001), ($\bar{2}$ 11), (220), (211) and (031) of monoclinic $SrAl_2O_4$. A minor peak is present at 32^0, indicating the $Sr_3Al_2O_6$ phase. Another peaks present at 19.55^0 and 27.97^0 indicates presence of another minor phase $Sr_7Al_{12}O_{25}$.

Rietveld refinement was carried out for the pure sample in the range 10^0 -90^0 using FullProf software. The refinement procedure confirmed the presence of a minor phase of tri strontium di aluminium hexoxide ($Sr_3Al_2O_6$). The phase fraction of the $SrAl_2O_4$ was 92.03%, while that of $Sr_3Al_2O_6$ was 7.97%. The global user-weighted Chi^2 value (Bragg contrib.) reached 3.38, R_{wp}=5.72, R_{exp}=3.11, and R_p=4.19(Fig. 2). The refinement values obtained are shown in Table 1.

Using the Scherrer equation, the average crystallite size of nanophosphors was determined [18].

$$D = \frac{k\lambda}{\beta cos\theta}$$

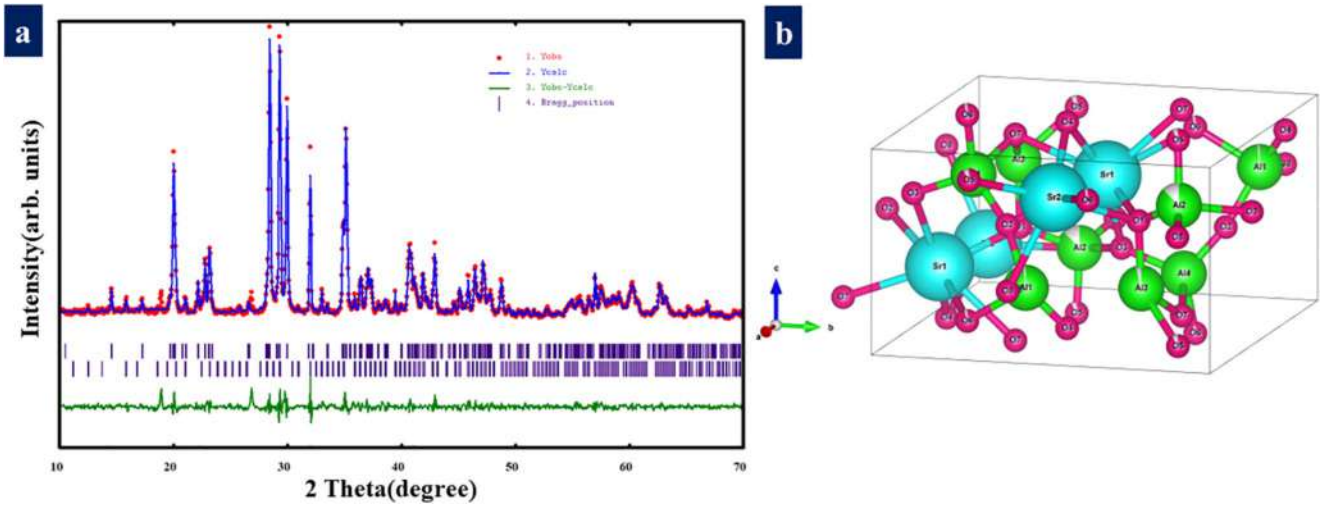

Fig. 2 (**a**) Rietveld refinement for the PXRD pattern of undoped $SrAl_2O_4$ (**b**) The crystal structure of $SrAl_2O_4$

Table 1 Results of Rietveld refinement

Phase	Cell Parameter	Direct Cell volume (Å^3)	Bragg R factor	Phase Fraction (%)	R_f factor
$SrAl_2O_4$	a = 8.444 Å b = 8.827 Å c = 5.154 Å α = 90^0 β = 93.37^0 γ = 90^0	383.5277	4.07	92.03	2.86
$Sr_3Al_2O_6$	a = 15.827 Å b = 15.827 Å c = 15.827 Å α = 90^0 β = 90^0 γ = 90^0	3965.099	8.15	7.97	4.75

For determining crystallite size, high intensity peaks corresponding to the planes ($\bar{2}$ 11), (220) and (211) peaks were selected. The calculated average crystallite size ranges from 45.23 nm to 42.07 nm as the Eu content increases from 0 at% to 3 at%(Table 2). The slight higher angle shift observed in the peaks of the doped samples, compared to the undoped sample, can be explained by the replacement of Sr^{2+} (1.21 Å) ions with smaller Eu^{3+} (1.01 Å) ions in the host lattice. This causes a reduction in the unit cell size, leading to the observed shift in the peaks.

The variance in ionic radius concerning the doped and substituting ions, termed acceptable percentage

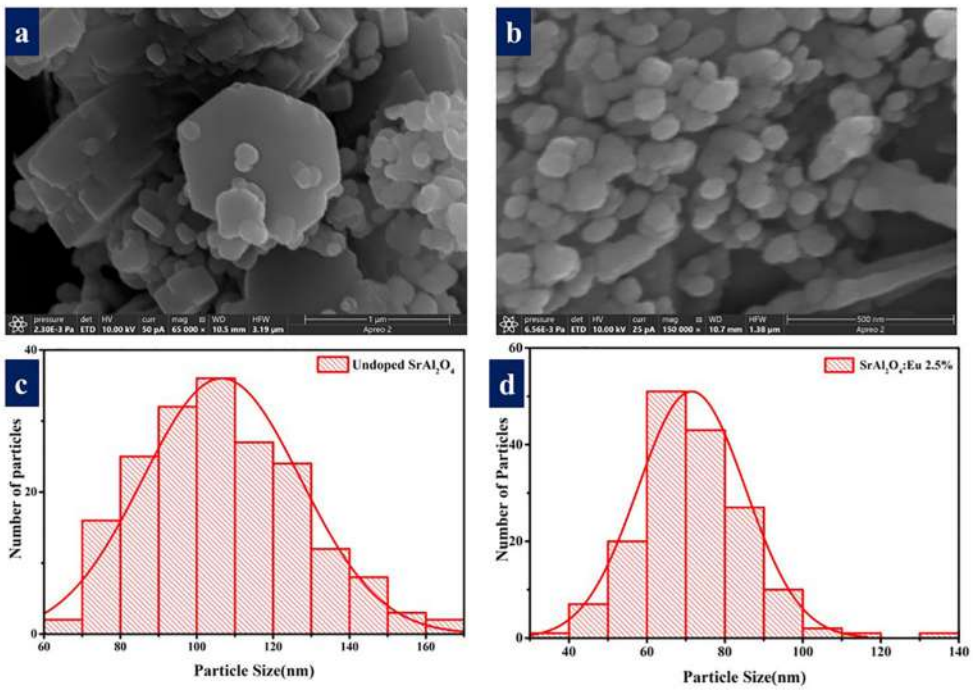

Fig. 3 SEM micrographs of $SrAl_2O_4$ with Europium concentration (**a**) Eu = 0 at% and (**b**) Eu = 2.5 at%. Particle size distribution of the spherical particles obtained for $SrAl_2O_4$ with Europium concentrations (**c**) Eu = 0 at% and (**d**) Eu = 2.5 at%

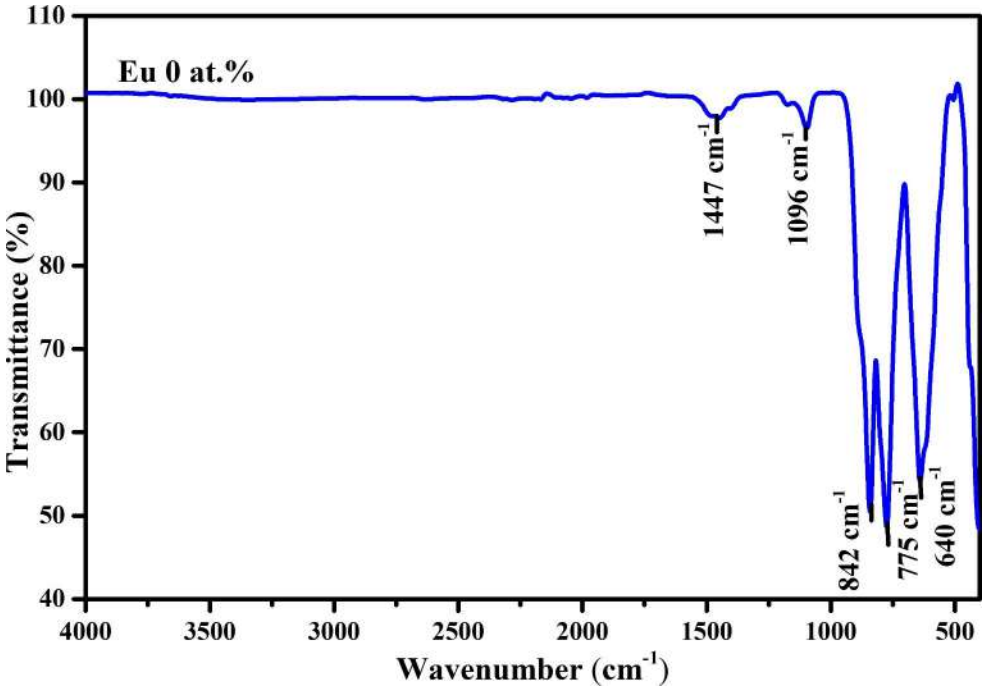

Fig. 4 FTIR spectra of host $SrAl_2O$

Table 2 Variation of crystallite size and band gap as a function of Eu doping concentration

Sl No.	Doping concentration of Eu^{3+} ions (at%)	Crystallite size (nm)	Band gap (eV)
1.	0	45	6.02
2.	0.5	44	5.89
3.	1.0	43	5.80
4.	1.5	42	5.67
5.	2.0	42	5.82
6.	2.5	42	5.69
7.	3.0	42	5.65

difference(D_r) should be less than 30% for the substitution to be permissible [19]. D_r is given by equation

$$D_r = \frac{R_s - R_d}{R_s}$$

where R_s and R_d are the ionic radii of host lattice ion(Sr^{2+}) and dopant ion (Eu^{3+})ions respectively. The estimated value of D_r as 16.5% which confirms that Eu^{3+} ions replace Sr^{2+}ions.

Scanning electron microscopy was employed to investigate the surface morphology of both the undoped sample and the sample containing 2.5% europium. Figure 3(a) and Fig. 3(b) depict the SEM micrographs obtained for the undoped sample and the sample containing 2.5% europium, respectively. The micrographs reveal that the undoped strontium aluminate particles exhibit a combination of spherical particles along with sheet like structures. Factors such as annealing temperatures and plane specific surface energy affect the relative growth in different direction and a shape change of particles is expected [20]. In contrast, the micrograph of the doped sample predominantly shows spherical particles along with some elongated rod like structures. The particle size analysis of the spherical particles was conducted using ImageJ software. It is obtained that the average

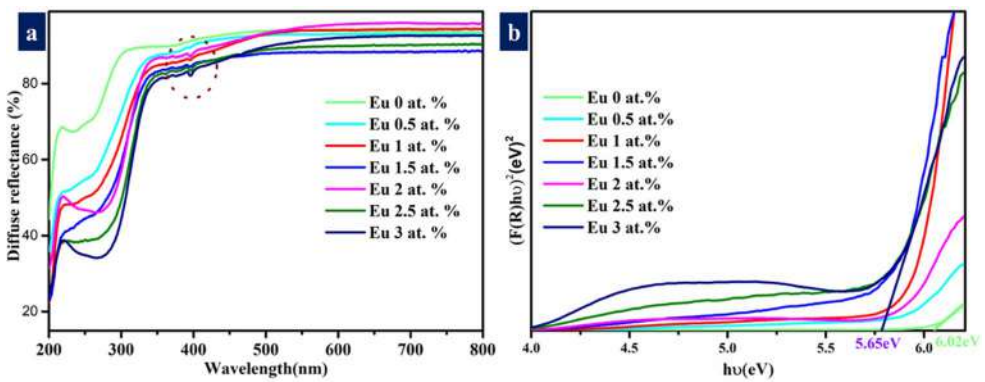

Fig. 5 (**a**) Diffuse reflectance spectra as a function of europium concentration (**b**) Band gap obtained for $Sr_{1-x}Al_2O_4$:xEu (x = 0 at% − 3 at%) nanophosphors

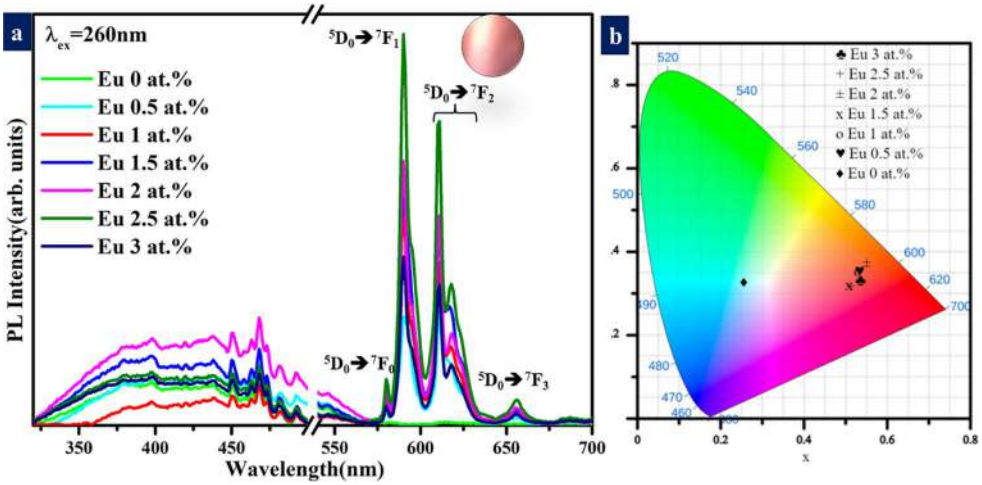

Fig. 6 (**a**) PL emission spectrum of Eu doped $SrAl_2O_4$ taken with excitation at 260 nm [inset]photo of emission from powder sample with doping concentration 2.5 at% (a break region is used to avoid the second harmonics of the excitation wave length) (**b**) CIE colour coordinates of europium doped materials

particle size of the spherical particles in the undoped sample is 99 nm (Fig. 3(c)) and the doped sample exhibits average particle size of 70 nm (Fig. 3(d)) similar to the observed variation in crystallite size.

FTIR spectroscopy was utilised to determine and analyse the functional groups present in the compound, providing insight into its chemical composition and structure. Figure 4 shows the FTIR spectrum of undoped $SrAl_2O_4$, acquired at room temperature from 4000 cm^{-1} to 400 cm^{-1}.The prominent peaks examined were 1447.53 cm^{-1}, 1096.76 cm^{-1}, 841.91 cm^{-1},775.07 cm^{-1}, 640.54 cm^{-1}.

The feeble peak at 1447.53 cm^{-1} indicates the negligible presence of $SrCO_3$, which is used as precursors of the synthesis [21]. Another peak at 1096 cm^{-1} is ascribed to the Al-O bond [22]. The intense peaks of the FTIR spectra of undoped $SrAl_2O_4$ in the fingerprint region are found at 841.91 cm^{-1} and 775.07 cm^{-1}, indicative of the Sr-O-Al and Al-O symmetric stretching vibrations, respectively, within the $SrAl_2O_4$ lattice [10, 22, 23]. The peak at 640.54 cm^{-1} corresponds to the anti-symmetric stretching vibrations of Sr-O bond [8, 24].

Optical Analysis

The experimental diffuse reflectance spectra (DRS) obtained for the $Sr_{1-x}Al_2O_4$:x Eu^{3+}(x = 0 at% − 3 at%) nanoparticles are displayed in the Fig. 5 (a). According to the spectra, it can be observed that all the samples demonstrate a significant level of transparency within the visible range. The reflection spectra for all the samples in the range 400 to 800 nm range remain qualitatively similar, regardless of the level of europium substitution. The absorption edge was observed at approximately 215 and 305 nm, a phenomenon that can be ascribed to the self-absorption band of the major phase $SrAl_2O_4$ (6.6 eV) and minor phase $Sr_3Al_2O_6$ (3.8 eV) respectively [25]. An inflexion point can be noticed at 397 nm, which intensifies as the concentration of Eu^{3+} increases; this absorption can be assigned to the $^7F_0 \rightarrow {}^5L_6$ transition of the dopant ions [25].

The band gap of material was determined by employing the Tauc plot method, which utilises the Kubelka-Munk function, a widely acknowledged technique for such computations [3, 26, 27]. Kubelka-Munk method uses the relation,

$$F(R) = \frac{(1-R)^2}{2R}$$

where R is the reflectance obtained from DRS spectroscopy, the plot of $(F(R)h\nu)^2$ versus hν is demonstrated in Fig. 5(b). The direct band gap of the pure $SrAl_2O_4$ sample was measured to be 6.02 eV, which is lower than the literature-reported value of 6.4 eV [27, 28]. Enhanced carrier-carrier interaction can cause a reduction (renormalisation) of the band gap by increasing the carrier concentrations in the conduction and valence bands [29]. It is found that the band gap decreases and reaches a value of 5.65 eV for the Eu concentration 3at.%.

Photoluminescence spectroscopy was used to investigate the impact of different concentrations of europium ions on the photoluminescence emission spectra of $Sr_{1-x}Al_2O_4$:xEu nanophosphors, as presented in Fig. 6(a). The intensity and colour richness of the emission spectra were evaluated by recording the spectra using an excitation wavelength of 260 nm.

The data outcome demonstrates that the luminescence intensity of $Sr_{1-x}Al_2O_4$:xEu nanophosphors rises with the concentration of Eu^{3+} ions up to an optimum level of 2.5 at.%. Beyond this, the intensity of luminescence reduces owing to the concentration quenching effect that arises from nonradiative energy transfer between neighbouring europium (III) ions [30, 31]. Figure 6(b) depicts the Commission Internationale de I' Eclairage (CIE) 1931 diagram of $Sr_{1-x}Al_2O_4$:xEu^{3+} nanoparticles. Table 3 shows the

Table 3 Variation of CIE coordinates with dopant concentration

Europium Concentration (in at%)	CIE Coordinates	
	x	y
0	0.25	0.32
0.5	0.53	0.35
1.0	0.53	0.35
1.5	0.51	0.31
2.0	0.55	0.37
2.5	0.51	0.31
3.0	0.53	0.33

calculated CIE colour coordinates (x, y) from the emission spectral measurements.

The local environment of Eu^{3+} can be probed by analysing the absorption and luminescence spectra of the ion. Spectroscopic data on the fine structure and relative transition intensities can reveal information on the Eu^{3+} site's point group symmetry and coordination polyhedron [25]. The prominent emission peaks are observed at 580 nm, 590 nm, 610 and 655 nm. The prepared materials have been observed to display unique emissions that can be attributed to the trivalent europium ion. These emissions arise from the $^5D_0 \rightarrow {}^7F_J$ transitions, where J takes 0, 1, 2, and 3 [32]. The peak at 610 nm is part of a doublet, with the second peak at 617 nm. This doublet formation is due to the occupancy of different strontium sites(Sr1) and (Sr2) sites by Eu^{3+}. It is worth noting that the most intense emission at a wavelength of 590 nm, observed across all europium concentrations, can be ascribed to $^5D_0 \rightarrow {}^7F_1$ magnetic dipole transition [33]. The highest intensity possessed by this transition is a direct manifestation of the centrosymmetric crystal structure of the material and is largely insensitive to the local environment surrounding the Eu^{3+} ion [25]. The f-f transitions of trivalent lanthanides are not significantly influenced by the presence of ligand ions in the host lattice, as most valence

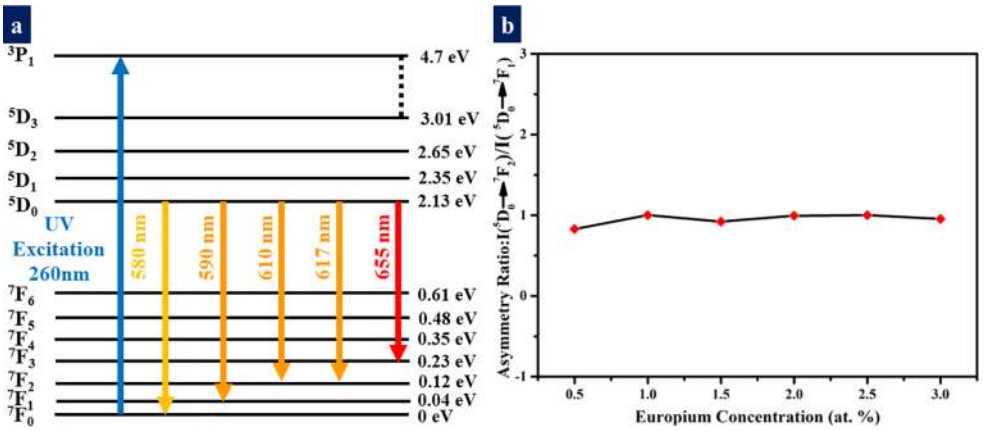

Fig. 7 (**a**) Energy level diagram showing transitions in Eu^{3+} ion in $Sr_{1-x}Al_2O_4$:xEu matrix (**b**) Variation of the asymmetry ratio in $Sr_{1-x}Al_2O_4$:xEu, when excited by 260 nm, with respect to the concentration of Eu^{3+} ions

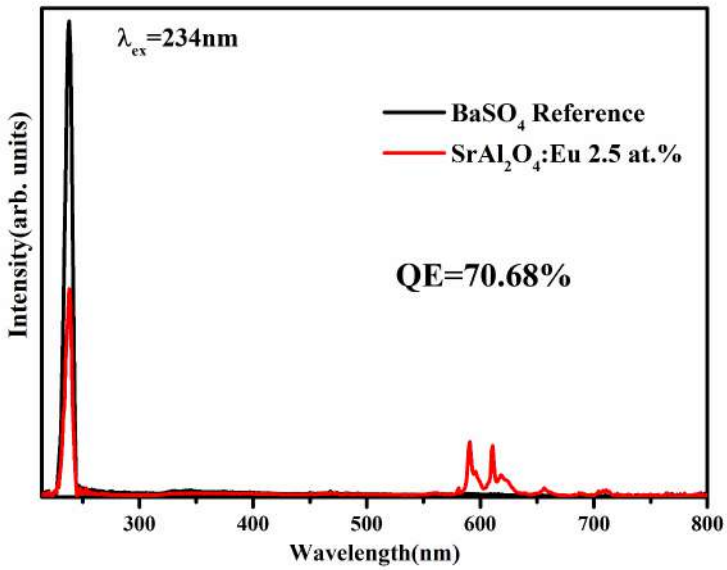

Fig. 8 Quantum efficiency of the $SrAl_2O_4$:Eu^{3+} (2.5 at%)phosphor

electrons are shielded by the outer electrons of 5s and 5p [31]. Consequently, the optical spectra of doped trivalent rare-earth elements in most phosphors show resemblances to those anticipated for unbound ions. Nonetheless, some transitions are susceptible to the crystal environment and are referred to as hypersensitive transitions. Peaks at 610 and 617 nm correspond to $^5D_0 \rightarrow {}^7F_2$ induced electric dipole transition, one of the hypersensitive transition of Eu^{3+}ion.

.

According to literature reports, if the Eu^{3+} site exhibits inversion symmetry, the emission strength of the electric dipole is weakened, resulting in the relatively greater strength of the magnetic dipole transition [7, 9]. As a result, the magnetic dipole transition tends to dominate in such a scenario. Thus the dominant emission obtained for the prepared nanophosphors for $^5D_0 \rightarrow {}^7F_1$ transition suggests that the Eu^{3+} site has an inversion centre. The energy level diagram Fig. 7(a) of europium ion illustrates the photoluminescence process.

The fraction of the intensities of $^5D_0 \rightarrow {}^7F_2$ transition to $^5D_0 \rightarrow {}^7F_1$ transition, referred to as the asymmetry ratio, can also be utilised to determine the extent of deviation from inversion symmetry within the local environment of the Eu^{3+} ion within a matrix [34, 35]. Figure 7 (b) shows the dependence of the asymmetry ratio on europium content in the crystal. It is found that the asymmetry ratio remains almost unchanged for all Eu^{3+} concentrations having an average value of 0.95.

Comparably lower peaks at 580 and 655 nm are ascribed to the $^5D_0 \rightarrow {}^7F_0$, and $^5D_0 \rightarrow {}^7F_3$ transition which are induced electric dipole transitions [25, 36]. A broad emission spectrum in the 300-500 nm range was found in undoped and doped samples. This is the combination of emissions from various defects from the host matrix. These intrinsic defects such as oxygen vaccancy (V_O), strontium vacancies (V_{Sr}), and certain colour centers [37, 38]. The absolute quantum efficiency of $SrAl_2O_4$:$_x$Eu (x = 2.5%) nanophosphor (excited at 234 nm) is 70.68% as shown in Fig. 8.

Conclusion

The present study reports stable orange red emitting europium-doped strontium aluminate polycrystalline nanophosphors using the solid-state reaction method. The obtained results from XRD and FTIR analysis confirmed the formation of $SrAl_2O_4$ phase with minor traces of $Sr_3Al_2O_6$. The direct band gap was determined to be 6.02 eV for undoped sample using Tauc plot. The photoluminescence study indicated bright orange-red emission with an optimal Eu concentration of 2.5 at%, exhibiting maximum peak intensity for the transition from $^5D_0 \rightarrow {}^7F_1$. The quantum efficiency for Eu 2.5 at% doped sample excited at 234 nm is 70.68%. These findings provide valuable insights into the electronic structure and optical properties of europium-doped strontium aluminate nanophosphors, highlighting their potential as highly efficient materials luminescent applications. The results of this study could pave the way for the development of next-generation luminescent materials with enhanced optical properties, opening up new avenues in the field of nanophotonics and nanomedicine.

Author Contributions All authors collectively contributed to the conception and design of the study. Anila E I and Neenu Mary Thomas were responsible for the conceptualization. Neenu Mary Thomas conducted the material preparation, data collection, and analysis. The initial draft of the manuscript was prepared by Neenu Mary Thomas, and E. I Anila provided valuable feedback, reviewed, and edited the manuscript. All authors have thoroughly read and approved the final version of the manuscript.

Funding The authors acknowledge instrumentation support of CLIF, Kerala University. The authors declare that no other funds, grants were received during the preparation of this manuscript.

Data Availability The datasets generated during and/or analyzed during the current study are not publicly available, but are available from the corresponding author on reasonable request.

Declarations

Competing Interests The authors declare no competing interests.

Ethics Approval This declaration is not applicable.

Consent to Participate This declaration is not applicable.

Consent to Publish This declaration is not applicable.

References

1. Van der Heggen D, Joos JJ, Feng A, Fritz V, Delgado T, Gartmann N, Walfort B, Rytz D, Hagemann H, Poelman D, Viana B, Smet PF (2022) Persistent luminescence in Strontium Aluminate: a Roadmap to a brighter future. Adv Funct Mater 32:2208809. https://doi.org/10.1002/adfm.202208809
2. Ju H, Liu J, Wang B, Tao X, Ma Y, Xu S (2013) Bi^{3+}-doped $Sr_3Al_2O_6$: an unusual color-tunable phosphor for solid state lighting. Ceram Int 39(1):857–860. https://doi.org/10.1016/j.ceramint.2012.05.106
3. Jamalaiah BC, Ramesh Babu Y (2018) Near UV excited $SrAl_2O_4$:Dy^{3+} phosphors for white LED applications. Mater Chem Phys 211:181–191. https://doi.org/10.1016/j.matchemphys.2018.02.025
4. Ashwini KR et al (2021) Green emitting $SrAl_2O_4$:Tb^{3+} nano-powders for forensic, anti-counterfeiting and optoelectronic devices. Inorg Chem Commun 130:108665. https://doi.org/10.1016/j.inoche.2021.108665. February
5. Benítez Guerrero NS, Rolón Rodríguez YM, Peña Rodríguez G (2046) "Use of strontium aluminate powders in the photocatalytic

removal of dyes present in water," *J. Phys. Conf. Ser*, vol. no. 1, pp. 0–6, 2021, https://doi.org/10.1088/1742-6596/2046/1/012042
6. Calatayud DG et al (2022) Biocompatible Probes based on rare-earth Doped Strontium Aluminates with long-lasting Phosphorescent Properties for in Vitro Optical imaging. Int J Mol Sci 23(6). https://doi.org/10.3390/ijms23063410
7. Zhang J, Zhang X, Shi J, Gong M (2011) Luminescent properties of green- or red-emitting Eu^{2+}doped $Sr_3Al_2O_6$ for LED. J Lumin 131(12):2463–2467. https://doi.org/10.1016/j.jlumin.2011.05.064
8. Wang L et al (2016) Enhancing photovoltaic performance of dye-sensitized solar cells by rare-earth doped oxide of $SrAl_2O_4:Eu^{3+}$. Mater Res Bull 76:459–465. https://doi.org/10.1016/j.materresbull.2016.01.013
9. Salehabadi A, Salavati-Niasari M, Gholami T (2018) Green and facial combustion synthesis of $Sr_3Al_2O_6$ nanostructures; a potential electrochemical hydrogen storage material. J Clean Prod 171:1–9. https://doi.org/10.1016/j.jclepro.2017.09.250
10. Rojas-Hernandez RE, Rodriguez MA, Fernandez JF (2015) Role of the oxidizing agent to complete the synthesis of strontium aluminate based phosphors by the combustion method. RSC Adv 5(4):3104–3112. https://doi.org/10.1039/c4ra10460a
11. Page P, Ghildiyal R, Murthy KVR (2006) Synthesis, characterisation and luminescence of $Sr_3Al_2O_6$ phosphor with trivalent rare earth dopant. Mater Res Bull 41(10):1854–1860. https://doi.org/10.1016/j.materresbull.2006.03.012
12. Vitola V et al (2020) The boron effect on low temperature luminescence of $SrAl_2O_4$:Eu, Dy. Ceram Int 46(16):26377–26381. https://doi.org/10.1016/j.ceramint.2020.01.208
13. Bierwagen J et al (2019) "Probing traps in the persistent phosphor $SrAl_2O_4:Eu^{2+},Dy^{3+},B^{3+}$ - A wavelength, temperature and sample dependent thermoluminescence investigation," *J. Lumin*, vol. 222, no. p. 117113, 2020, https://doi.org/10.1016/j.jlumin.2020.117113
14. Vitola V, Millers D, Smits K, Bite I, Zolotarjovs A (2019) "The search for defects in undoped $SrAl_2O_4$ material," *Opt. Mater. (Amst)*, vol. 87, no. February, pp. 48–52, https://doi.org/10.1016/j.optmat.2018.06.004
15. Zhang P, Li L, Xu M, Liu L (2008) The new red luminescent $Sr_3Al_2O_6:Eu^{2+}$ phosphor powders synthesized via sol-gel route by microwave-assisted. J Alloys Compd 456:1–2. https://doi.org/10.1016/j.jallcom.2007.02.004
16. Sanad MMS, Rashad MM (2016) Tuning the structural, optical, photoluminescence and dielectric properties of Eu^{2+}-activated mixed strontium aluminate phosphors with different rare earth co-activators. J Mater Sci Mater Electron 27(9):9034–9043. https://doi.org/10.1007/s10854-016-4936-0
17. Kostova MH, Zollfrank C, Batentschuk M, Goetz-Neunhoeffer F, Winnacker A, Greil P (2009) Bioinspired design of $SrAl_2O_4:Eu^{2+}$ phosphor. Adv Funct Mater 19(4):599–603. https://doi.org/10.1002/adfm.200800878
18. Patterson AL (1939) The scherrer formula for X-ray particle size determination. Phys Rev 56(10):978–982. https://doi.org/10.1103/PhysRev.56.978
19. Pires AM, Davolos MR (2001) Barium and Zinc Orthosilicate. Chem Mater 13(1):21–27
20. Wei KongBoLiuBoYeZhongpingYuHua (2011) Wang,Guodong Qian,and Zhiyu Wang,"An Experimental Study on the Shape Changes of TiO_2 Nanocrystals Synthesized by Microemulsion-Solvothermal Method. J ofNanomaterials Volume 467083. https://doi.org/10.1155/2011/467083
21. Chroma M, Pinkas J, Pakutinskiene I, Beganskiene A, Kareiva A (2005) Processing and characterisation of sol-gel fabricated mixed metal aluminates. Ceram Int 31(8):1123–1130. https://doi.org/10.1016/j.ceramint.2004.11.012
22. Zhu Y, Zheng M, Zeng J, Xiao Y, Liu Y (2009) Luminescence enhancing encapsulation for strontium aluminate phosphors with phosphate. 113:721–726. https://doi.org/10.1016/j.matchemphys.2008.08.007
23. Singh V et al (2009) Characterisation, luminescence and EPR investigations of Eu^{2+} activated strontium aluminate phosphor. J Non Cryst Solids 355:50–51. https://doi.org/10.1016/j.jnoncrysol.2009.08.027
24. Li Z, Hao S, Ji W, Hao L, Yin L, Xu X (2021) Mechanism of long afterglow in $SrAl_2O_4$: Eu phosphors. Ceram Int no August. https://doi.org/10.1016/j.ceramint.2021.08.193
25. Binnemans (2015) "Interpretation of europium(III) spectra", Coordination Chemistry Reviews, Volume 295, Pages 1–45, ISSN 0010-8545, doihttps://doi.org/10.1016/j.ccr.2015.02.015
26. Escobedo-Morales A, Ruiz-López II, Ruiz-Peralta MdeL, Tepech-Carrillo L, Sánchez-Cantú M, Moreno-Orea JE (2019) Automated method for the determination of the band gap energy of pure and mixed powder samples using diffuse reflectance spectroscopy. Heliyon 5(4):1–19. https://doi.org/10.1016/j.heliyon.2019.e01505
27. Fu Z, Zhou S, Pan T, Zhang S (2005) Band structure calculations on the monoclinic bulk and nano-$SrAl_2O_4$ crystals. J Solid State Chem 178(1):230–233. https://doi.org/10.1016/j.jssc.2004.11.032
28. Hölsä J, Laamanen T, Lastusaari M, Niittykoski J, Novák P (Aug. 2009) Electronic structure of the $SrAl_2O_4:Eu^{2+}$ persistent luminescence material. J Rare Earths 27(4):550–554. https://doi.org/10.1016/S1002-0721(08)60286-0
29. Piprek J (2003) "Electron Energy Bands," *Semicond. Optoelectron. Devices*, pp. 13–48, https://doi.org/10.1016/b978-0-08-046978-2.50027-2
30. Dexter DL, Schulman JH (1954) Theory of concentration quenching in inorganic phosphors. J Chem Phys 22:1063–1070. https://doi.org/10.1063/1.1740265
31. Safeera TA, Anila EI (2018) "Synthesis and characterization of $ZnGa_2O4:Eu^{3+}$ nanophosphor by wet chemical method",Scripta Materialia, Volume 143, Pages 94–97, ISSN 1359–6462, doi.: https://doi.org/10.1016/j.scriptamat.2017.09.021
32. López R, Gómez R (2012) Band-gap energy estimation from diffuse reflectance measurements on sol-gel and commercial TiO_2: a comparative study. J Sol-Gel Sci Technol 61(1):1–7. https://doi.org/10.1007/s10971-011-2582-9
33. Bindu KR, Safeera TA, Anila EI (2022) Pure red luminescence and concentration-dependent tunable emission color from europium-doped zinc sulfide nanoparticles. J Mater Sci: Mater Electron 33:17793–17801. https://doi.org/10.1007/s10854-022-08644-5
34. Nogami M, Enomoto T, Hayakawa T (2002) Enhanced fluorescence of Eu^{3+} induced by energy transfer from nanosized SnO_2 crystals in glass. J Lumin 97:3–4. https://doi.org/10.1016/S0022-2313(02)00217-X
35. Tsai BS, Chang YH, Chen YC (2005) Synthesis and luminescent properties of $MgIn_{2-x}Ga_xO_4Eu^{3+}$ phosphors. Electrochem Solid-State Lett 8(7):55–57. https://doi.org/10.1149/1.1921128
36. Rekha S, Anila EI (2019) Intense yellow emitting Biocompatible CaS:Eu Nanophosphors synthesized by Wet Chemical Method. J Fluoresc 29:673–682. https://doi.org/10.1007/s10895-019-02375-3
37. Huang YM, Ma Qing-lan (2015) Long afterglow of trivalent dysprosium doped strontium aluminate. J Lumin 160:271–275. https://doi.org/10.1016/j.jlumin.2014.12.042
38. Thomas NM, Sreeja VG, Vanchipurackal IV, Anila EI (2020) Structural and linear optical properties of blue light emitting $Sr_3Al_2O_6$. AIP Conf Proc 2265:030141. https://doi.org/10.1063/5.0016980